Electron-Only Tail Current Sheets and Their Temporal Evolution

M. Hubbert[1], Yi Qi[1], C.T. Russell[1], J.L. Burch[2], B.L. Giles[3], T.E. Moore[3]

[1]Earth Planetary and Space Sciences, University of California Los Angeles, Los Angeles, CA 90095-1567.

[2]Southwest Research Institute, San Antonio, TX 78238.

[3]Goddard Space Flight Center, NASA, Greenbelt, MD 20771.

Corresponding author: Mark Hubbert (mhubbert@epss.ucla.edu)

Key Points:

- 11 electron-only reconnection events observed by MMS in the near-Earth magnetotail
- Three events are snapshots in a time evolution into "electron-ion" reconnection
- Five events occur after "electron-ion" reconnection; Electron-only reconnection is more than a precursor to "electron-ion" reconnection

Abstract

The Earth's magnetotail contains a current sheet separating the anti-Sunward field of the southern lobe from the sunward-pointing northern lobe. Herein, we report tail current sheets that are supported by only electron currents. We examine one electron-only current sheet in detail, and briefly discuss ten others. Three current sheets are interpreted in terms of the time-evolution of reconnection onset. These current sheets show evidence of parallel electron heating, perpendicular ion heating, and current sheet expansion. These features are consistent with electron and ion behavior during traditional "electron-ion" reconnection. Ground-based and in-situ data show that electron-ion reconnection occurs shortly after each "pre-ion reconnection" electron-only reconnection event. This suggests that electron-only reconnection can act as a precursor to electron-ion reconnection. We note that five events occur shortly after a period of electron-ion reconnection, which suggests that electron-only reconnection is more than merely a precursor to ion reconnection.

Plain Language Summary

Magnetic reconnection is a key process in conversion of magnetic energy to kinetic and thermal energy in space and laboratory plasmas. The Magnetosphere Multiscale (MMS) mission is designed to study the physics of magnetic reconnection with unparalleled time and spatial resolution. In this letter, we present several MMS observations of electron-supported current sheets that do not show signatures of typical magnetic reconnection, dubbed "Electron-Only" reconnection. We use three events to show that "electron-only" reconnection can lead to "electron-ion" magnetic reconnection. We use six events to suggest that "electron-only" reconnection occurs in more regimes than merely during the onset of "electron-ion" reconnection.

1 Introduction

Magnetic reconnection is a fundamental plasma process that converts magnetic energy into kinetic and thermal energy in laboratory and space plasmas [Dungey, 1961; Yamada et al., 2010]. Inside the ion diffusion region (IDR), the curvature of the magnetic field approaches the gyroradius of ions, causing ion trajectories to deviate from simple gyromotion. Closer to the reconnection point, in the electron diffusion region (EDR), electrons in tighter gyro-orbits transition to more chaotic orbits [Fu et al., 2006]. These two components of the reconnection region allow ions and electrons to be demagnetized, energized, and ejected in jets directed outward [Pritchett, 2001, Oka et al., 2016], but because of their different masses, these regions are often well separated [Sonnerup et al., 1979]. This process can establish a dynamic equilibrium in the magnetosphere. While the maintenance of the currents is a shared responsibility between electrons and protons, a plasma can have charge neutrality and current supplied primarily by electrons. This paper identifies 11 occasions when this occurred in the Earth's magnetotail.

Recently, using the high time and spatial resolution of the Magnetosphere Multiscale (MMS) Mission, several observers have reported a phenomenon dubbed "electron-only" reconnection in various magnetic environments [Phan et al., 2018, Wang et al., 2018, Stawarz et al., 2019]. These observations meet every observational criteria for an EDR except the ion response one might expect in traditional magnetic reconnection [Phan et al., 2018]. Two mechanisms have been proposed for this process: low frequency, high amplitude waves (specifically below the lower hybrid frequency) [Vega et al., 2020, Wang et al., 2018], and the current sheet having a small length (in the L direction) to width (in the M direction) ratio [Mallett, 2019, Pyakurel et al., 2019]. However, due to few observations and the disparate nature and rarity of "electron-only" reconnection, a consensus on their origin or nature has not yet been established.

We have surveyed MMS data in the near-Earth magnetotail during Phases 2B and 3B, and report on a set of electron-only reconnection observations in the tail current sheet. We examine one case in detail, put three events in "time sequence", and discuss the remaining events briefly. We also analyze ground and satellite data surrounding these events to confirm that electron-only reconnection can occur both before and after traditional ion reconnection. This investigation of electron-only reconnection helps to establish its nature and better understand its role in the dynamics of space plasma.

2 Instrumentation

This paper uses measurements from the MMS mission, a constellation of four identical, well-instrumented spacecraft, flying in a tetrahedron formation [Burch et al, 2016]. Magnetic field data were obtained at a time resolution of 128 Hz from the Flux Gate Magnetometer (FGM) [Russell et al., 2014], and plasma data were obtained at time resolutions of 150 ms (ions) and 30 ms (electrons) from the Fast Plasma Instrument (FPI) [Pollock et al., 2016]. Electric field data at a time resolution of 8192 Hz were provided by the Electric Field Double Probe (EDP) [Ergun et al., 2016; Lindqvist et al., 2016]. The average spacecraft separation in our 11 events is approximately 25 km. All data in this paper are taken from the MMS2 spacecraft because observations are identical across the four spacecraft and are presented in Geocentric Solar Magnetospheric (GSM) coordinates unless stated otherwise.

3 Observations of Electron-Only Current Sheets

On June 17, 2017, from 20:24:00-20:24:30, MMS was located at [X: -19.3, Y: -10.3, Z: 5.5] R_E (GSM) and crossed the near-Earth plasma sheet from the southern lobe to the northern lobe. The local coordinate system is: L: [0.948,0.315,-0.049], M: [-0.149,-0.304,0.934], N: [0.180,-0.926,-0.330] with respect to GSM coordinates. We determine the normal direction (N) using the four-spacecraft timing method [Russell et al., 1983]. The L direction is the direction of the field in the northern lobe averaged with the negative of the field in the southern lobe. The M-component is N x L. In Figure 1, FPI v_e components (Fig. 1c), $T_{i,\parallel}, T_{i,\perp}, T_{e,\parallel}$, and $T_{i,\perp}$ (Fig. 1f,g) are smoothed using a 3-point running average. B and E components (Fig. 1a,d) are averaged to FPI v_e cadence, then smoothed using a 3-point running average. FPI n_e is averaged to match the time resolution of FPI n_i (Fig. 1e). Energy conversion (Fig. 1h) is calculated using $J \cdot E'$ $(E' = E + v_e \times B)$, where J is the four-spacecraft average of the current density using FPI plasma moments $(J = en_e(v_i - v_e))$ and E' uses the four-spacecraft averages of EDP electric field, FPI v_e, and FGM magnetic field. We calculate the expected $E \times B$ drift velocity ($v_{E\times B}$, Fig. 1i,j,k) using $\frac{E\times B}{B^2}$, where E and B are the measured electric and magnetic field vectors, respectively. Electric field data are averaged to magnetic field cadence to perform the calculation, then the resulting vector is averaged to FPI v_e cadence and smoothed using a 3-point running average. We then compare $v_{E\times B}$ to the perpendicular electron velocity ($v_{e,\perp}$), which is calculated as $-\frac{(v_e\times B)\times B}{B^2}$.

This interval displays several criteria for identifying electron-only reconnection. At ~20:24:07.1, when B_L approaches 0, MMS2 observes an absolute minimum in B_{tot} (Fig. 1a), super-Alfvenic v_{eL} (Fig. 1c) and no super-Alfvenic v_{iL} (Fig. 1b). This system's geometry generates strong B_L and E_N (Fig. 1a,d). n_i and n_e (Fig. 1e) are equal within FPI uncertainty, indicating that the electrons are primarily carrying the current [Huang et al., 2018]. Far from the current sheet, $T_{e,\parallel}$ exceeds $T_{e,\perp}$ (Fig. 1g), but as MMS2 approaches the current sheet center, both directions are energized, and T_e becomes more isotropic. This is consistent with previously observed EDR crossings during "electron-ion" reconnection in the near-Earth magnetotail [Chen et al., 2019, Li et al., 2019, Zhou et al., 2019]. However, $T_{i,\perp}$ only slightly exceeds $T_{i,\parallel}$ (Fig. 1f) and does not vary during current sheet crossing. During a typical magnetotail EDR crossing, $T_{i,\perp}$ significantly exceeds $T_{i,\parallel}$ [Zhou et al., 2019]. $J\cdot E'$ (Fig. 1h) is significant and positive near the current sheet center. This is consistent with electrons gaining energy from the annihilating fields [Torbert et al., 2018]. Fig. 1i, j, and k compare each component of $v_{e,\perp}$ and $v_{E\times B}$. Deviation of $v_{e,\perp}$ from $v_{E\times B}$ close to the current sheet center (20:24:06.7 – 20:24:07.3) shows that electrons became demagnetized in this region [Torbert et al., 2018]. Lastly, MMS2 observed a crescent distribution in the $v_{e\perp 1}-v_{e\perp 2}$ plane (Fig. 1l) and strong wave activity near the lower hybrid frequency in both magnetic (Fig. 1m) and electric field (Fig. 1n) power spectra. These features suggest that MMS crossed a current sheet supported mostly by electrons inside which the electrons were demagnetized and energized due to annihilating magnetic field, but ions were mostly unaffected, justifying the terminology "electron-only reconnection" for this event.

We note that, for this event, MMS's trajectory was directed primarily in the N direction [Wang et al., 2019], which may complicate observation of ion response. However, MMS observes the same features described above during more traditional trajectories in Events #1 & 3 in Table 1 (See Supplementary Materials, Figs. SM1 & 2). This suggests that the lack of ion response is not an artifact of MMS's trajectory.

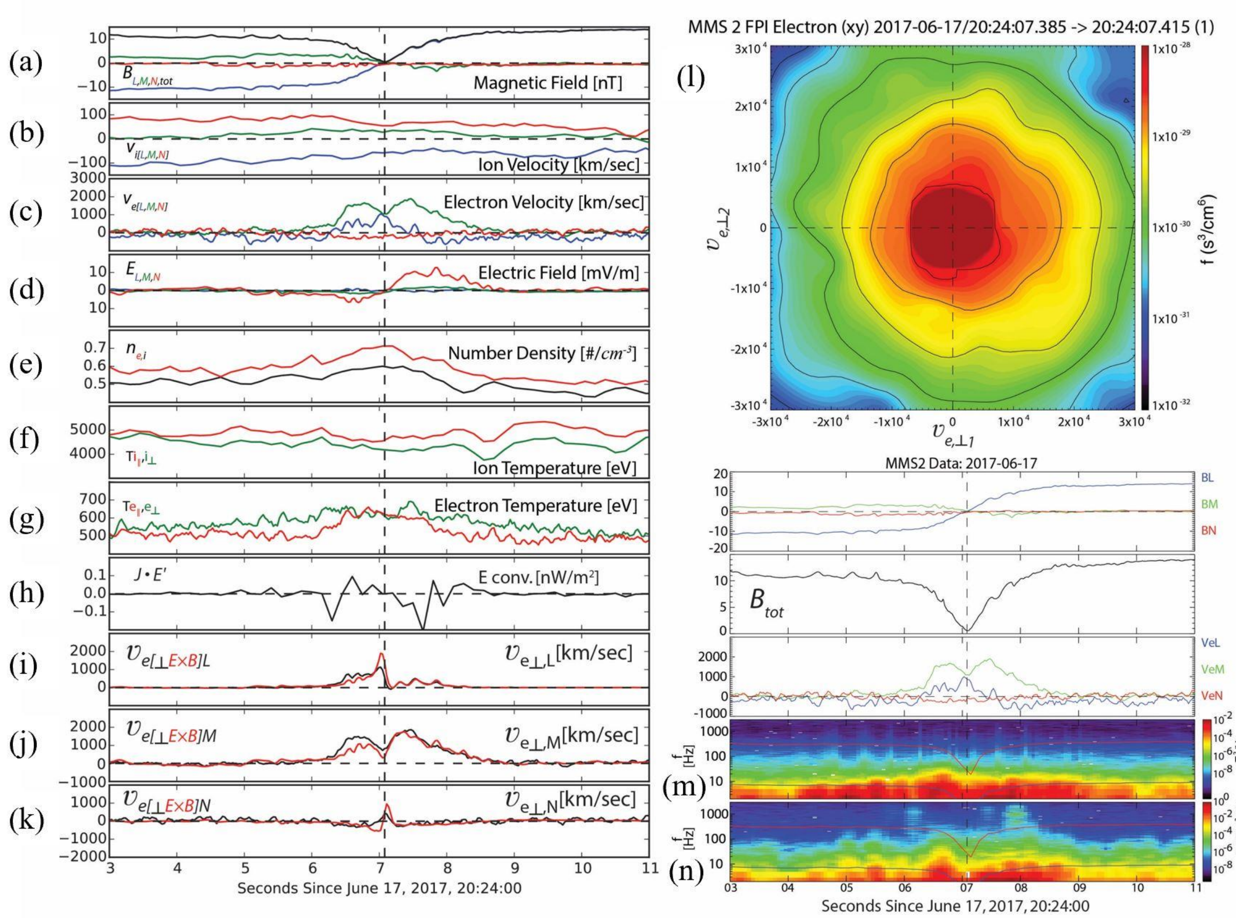

Figure 1: Event #2 in Table 1. (a) B components (L: Blue, M: Green, N: Red) and magnitude (black), (b) v_i bulk flow components, (c) v_e bulk flow components, (d) E components, (e) n_e (red) and n_i (black), (f) $T_{i,\perp}$ (red) and $T_{i,\parallel}$ (green), (g) $T_{e,\perp}$ (red) and $T_{e,\parallel}$ (green), (h) $J \cdot E'$, (i,j,k) $v_{e,\perp}$ (black) and $v_{E\times B}$ (red) components, (l) Perpendicular electron velocity distribution ($v_{e,\perp 1} = \frac{(B\times v_e)\times B}{B^2}, v_{e,\perp 2} = \frac{B\times v_e}{B}$), (m,n) magnetic and electric field power spectra (Red line is electron cyclotron frequency w_{ce}. Blue line is lower hybrid frequency w_{LH}.

Using the features described in Figure 1, we have identified ten more MMS observations of electron-only reconnection in the near-Earth magnetotail. Specifically, we used the following criteria: 1. Current Sheet Crossing (B_L reversal), 2. Absolute minimum in B_{tot}, 3. Lack of ion exhaust jets ($v_{iL} < v_{iA}$, no v_{iL} reversal), 4. Super-Alfvenic electron exhaust jets ($v_{eL} > v_{iA}$), 5. Lack of significant T_i response, 6. Significant T_e energization, 7. Positive $J \cdot E'$, and 8. Deviation of $v_{e\perp}$ from $v_{E\times B}$.

		CS	Normal	Dir			MMS	Loc.	
#	**Time Interval**	**X**	**Y**	**Z**	**Thick. (km,d_e)**	**Vel. (km/sec)**	**X**	**Y**	**Z**
1	*7-20-17/09:59-10*	*0.36*	***0.88***	*-0.29*	*77, 9.3*	*77*	*-21.6*	*7.9*	*1.3*
2	*6-17-17/20:24-25*	*0.18*	***-0.925***	*-.33*	*69, 10*	*69*	*-19.3*	*-11.1*	*3.5*
3	*6-19-17/09:43-44*	*0.08*	*0.24*	***-.966***	*219, 14.6*	*73*	*-20.5*	*-2.0*	*3.14*

4	6-13-17/21:09-10	-0.01	0.35	**0.94**	860, 86	172	-20.9	-5.6	1.9
5	7-06-17/05:38-39	0.082	-.571	**-.816**	186, 29	31	-20.7	3.3	2.7
6	7-24-17/13:04-05	0.22	**-.788**	0.57	294, 21	294	-18.4	1.9	5.0
7	7-26-17/17:39-40	0.65	**0.75**	0.03	852, 72	284	-23.5	6.4	4.6
8	8-07-17/11:04-05	0.07	0.47	**0.88**	410, 39	82	-19.1	6.9	2.8
9	7-23-18/15:04-05	0.41	-0.34	**0.84**	100, 8.4	10	-17.4	6.1	4.4
10	7-26-18/13:05-06	-0.58	**0.725**	-0.36	720, 60	120	-18.7	7.0	4.2
11	8-01-18/12:58-59	0.35	**0.87**	0.348	190, 40	38	-22.2	7.9	4.8

Table 1. Event Number (Column 1), Time Interval (Column 2), Current Sheet Normal Orientation in XYZ GSM (Column 3-5), Current Sheet Thickness (Column 6), Current Sheet Normal Speed (Column 7), and MMS Spacecraft Location in XYZ GSM (Column 8-10) for each Electron-Only Reconnection Observation. Bolded component of current sheet normal orientation is dominant component for corresponding event. Bolded Event #'s indicate "pre-ion reconnection" electron-only events. Italicized events display the time evolution of reconnection onset in Section 4.

Times and locations of these events are given in Table 1. Events in this paper were found during MMS Phase 2B (June-August 2017) and 3B (June-August 2018), when MMS was in the low-latitude magnetotail with an apogee of ~25 RE. Using the four-spacecraft timing method [Russell et al., 1983] on the B_x measurement, we calculated the current sheet normal orientation, speed, and thickness. Calculated normal directions and speeds are consistent over the entire crossing. We calculate current sheet thickness by determining the temporal width of the perpendicular current over the interval and multiplying it by the current sheet normal speed. This thickness in km is converted to electron inertial lengths (d_e) using the upstream electron number density ($d_e = c * \left(\frac{4\pi n_e e^2}{m_e}\right)^{-\frac{1}{2}}$). 2D projections of each event's location, current sheet normal velocity, and current sheet thickness (See Table 1) are plotted in Figure 2. In the XY plane, the current sheet center is rotated to account for solar wind aberration due to Earth's orbit. 2D projections of current sheet normal velocity are presented as arrows whose midpoints are fixed at the event location (Fig. 2a,c). An arrow's length and direction indicate a 2D projection of the current sheet normal speed and orientation, respectively. The shade of each event (Fig. 2b,d) indicates its current sheet thickness in d_e.

These events appear in both the dawn and dusk sectors (Fig. 2a,b), and are all located in positive GSM Z (Fig. 2c,d). We attribute this to MMS spending almost all its dwell time in positive GSM Z during Phases 2B and 3B. These events are typically composed of slow (≤ 120 km/sec) current sheets split evenly in orientation between GSM Y and Z (See Table 1). No current sheets are moving primarily in the GSM X direction. Events range in thickness from sub-ion scale (~8 d_e) to ion scale (~86 d_e), indicating that these thin current sheets need not be sub-d_i to occur.

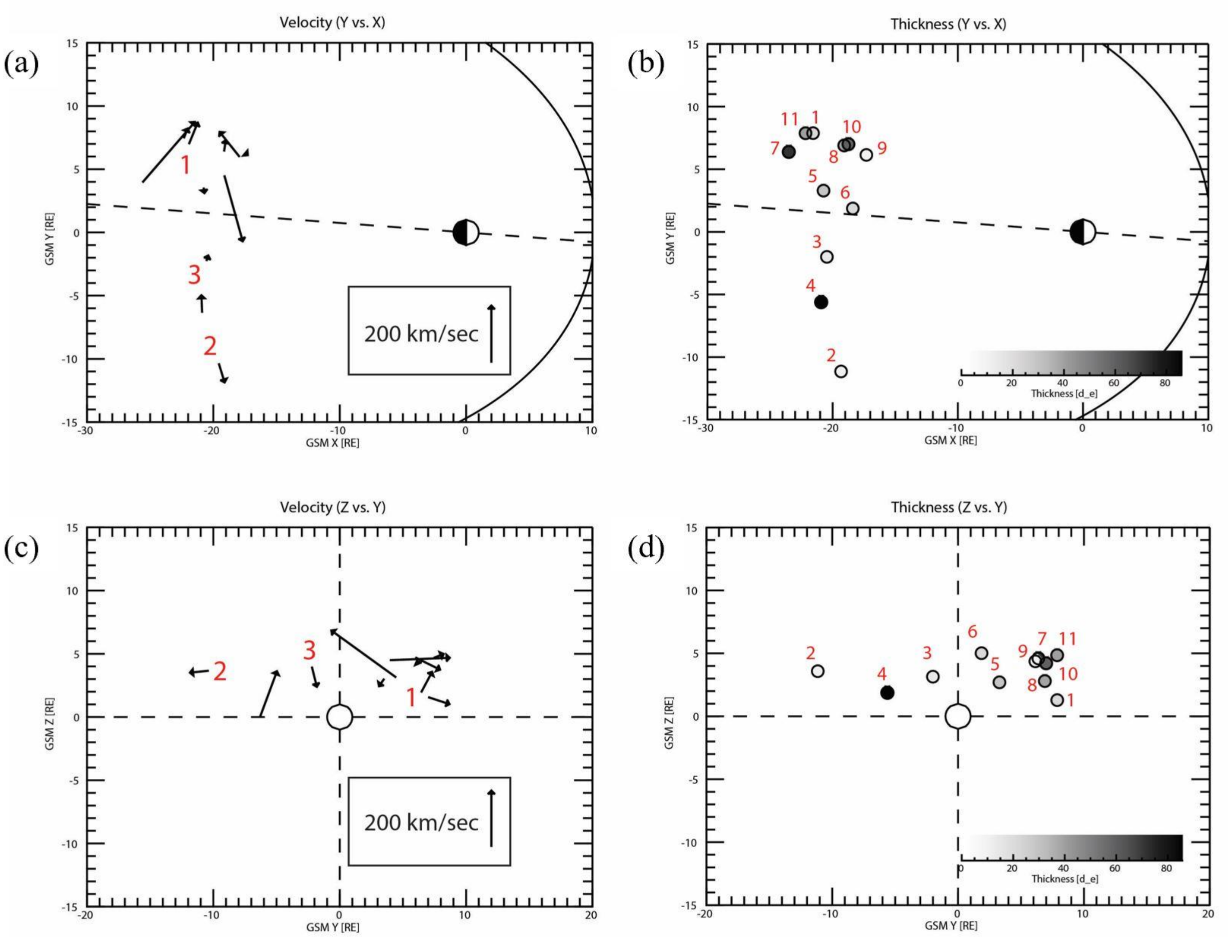

Figure 2: Projection of event locations, current sheet normal orientation (arrow direction), and current sheet normal speed (arrow length) onto (a) the XY GSM plane, and (b) the YZ GSM plane. Projection of event locations (point) and current sheet thickness in d_e (Shading) onto (c) the XY GSM plane and (d) the YZ GSM plane. Boxed arrows in panels (a,c) are references indicating the arrow length for a speed projection of 200 km/sec. Dashed lines in panels (a,b) are the aberration of solar wind due to Earth's orbital motion. Arrows labeled in panels (a,c) are the three events used to postulate the time evolution of Electron-Only Reconnection in Section 4.

An important question is the relation of electron-only events to traditional electron-ion reconnection. Thus, we have surveyed MMS data and ground geomagnetic data for "electron-ion" reconnection signatures within sixty minutes prior to and following electron-only observations. To classify reconnection signatures in geomagnetic data, we require significant perturbation in the AE index within sixty minutes of the event observation. To classify reconnection signatures in MMS data, we require a B_L reversal (current sheet crossing), B_{tot} minimum, super-Alfvenic v_{iL}, and a T_i increase (ion energization). If MMS and AE index signatures conflict, MMS signatures takes priority. Five events displayed reconnection signatures following the electron-only interval (Events #1-5, Table 1) and will be called "pre-ion reconnection" events throughout the paper. Five events displayed reconnection signatures prior to the electron-only interval (Events #6-8,10,11, Table 1). One event showed no reconnection signature before or after (Event #9, Table 1), indicating that the X-point did not move across MMS.

4 Time Evolution of Electron-Only Reconnection During Reconnection Onset

We now use three “pre-ion reconnection” electron-only events (Event #1 (t_1), Event #2 (t_2), and Event #3 (t_3) [Yu et al., 2019], italicized in Table 1) and one EDR crossing during well-developed reconnection observed by MMS in the near-Earth magnetotail to describe the evolution of electron-only reconnection during “electron-ion” reconnection onset. Overview plots of Event #1 and 3 structured identically to Figure 1 are available in the Supplementary Materials (Fig. SM1,2). Features of a traditional EDR crossing were taken from MMS observations of the interval 08-10-2017/12:18-19 [Li et al., 2019, Zhou et al., 2019]. The electron-only events are thin ($\leq 21\ d_e$), slow (≤ 100 km/sec) current sheets [Forbes et al., 1981] with varied current sheet normal orientations (two in Y, one in Z). All three current sheets are moving in the Earthward direction, consistent with the buildup phase of energy in the magnetotail. Most importantly, all three events are followed by traditional reconnection within 10 minutes after each current sheet crossing. Specifically, the AE Index displays significant (>100%) growth within 10 minutes after Event #2 (t_2) (Fig. 3a-c). In addition, MMS observes electron-ion reconnection signatures less than 10 minutes following Event #1 (t_1) and Event #3 (t_3) (See Supplementary Materials, Fig. SM3).

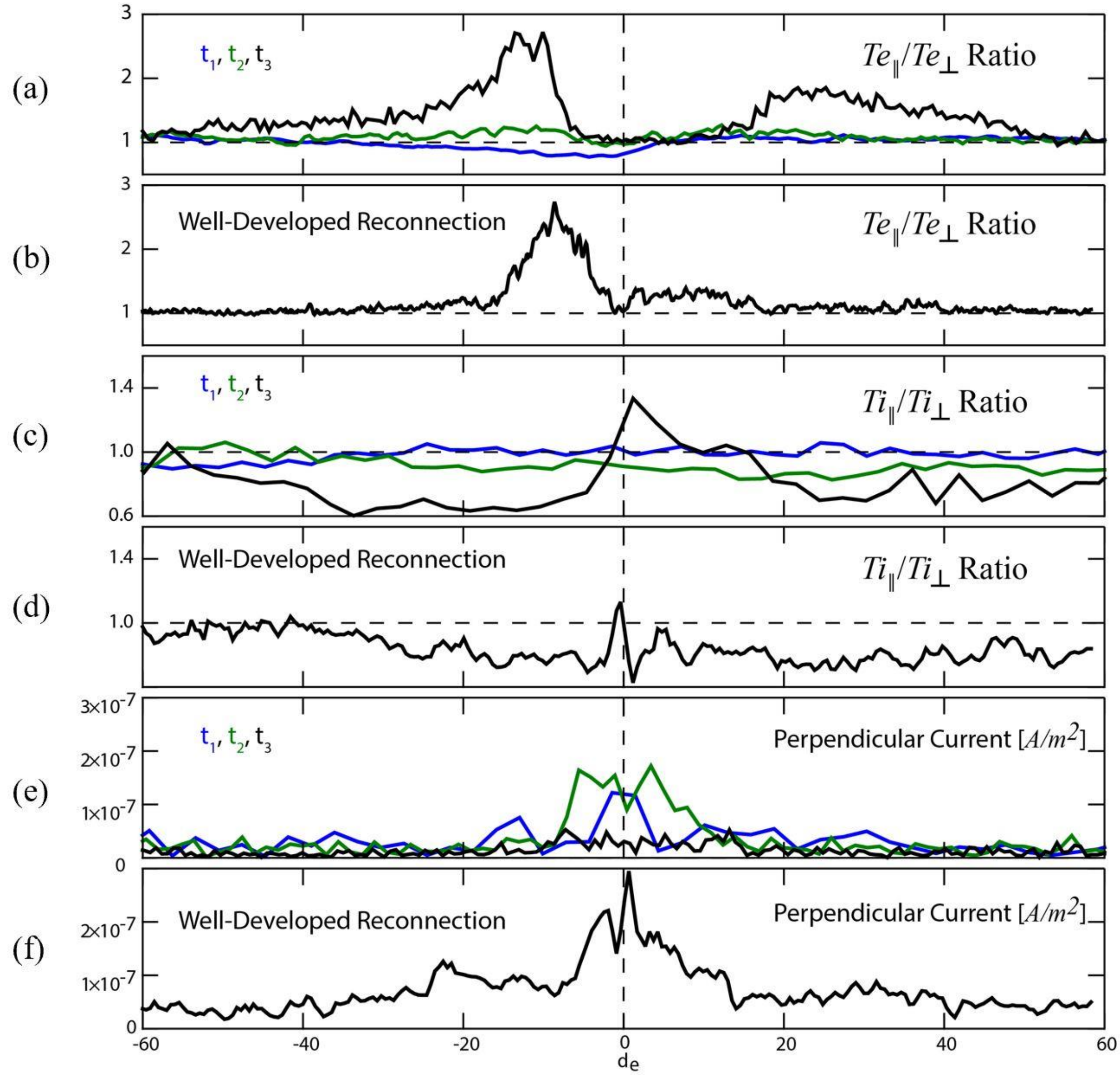

Figure 3: Comparison of early-phase of Electron-Only Reconnection (Events #1-3) with well-developed reconnection (08-10-2017/12:18-19). (a) $T_{e,\parallel}/T_{e,\perp}$ for Event #1 (t_1, Blue), Event #2 (t_2, Green), and Event #3 (t_3, Black) with respect to current sheet center, (b) $T_{e,\parallel}/T_{e,\perp}$ during well-developed EDR crossing in the magnetotail, (c) $T_{i,\parallel}/T_{i,\perp}$ for Event #1 (t_1, Blue), Event #2 (t_2, Green), and Event #3 (t_3, Black), (d) $T_{i,\parallel}/T_{i,\perp}$ during well-developed EDR crossing in the magnetotail, (e) Perpendicular Current for Event #1 (t_1, Blue), Event #2 (t_2, Green), and Event #3 (t_3, Black), (f) Perpendicular Current during well-developed EDR crossing in the magnetotail.

To compare the features of these events, we convert time to distance from the current sheet center using the method described earlier. We first indicated the temporal current sheet center of each event using the time at which B_{tot} reached its minimum value. We then converted time separation into d_e the same way we calculated current sheet thickness. The “distance” resolution of each line was then averaged to match the distance resolution of the lowest resolution array. Presenting the data in this format allows current sheet properties to be compared one-to-one, regardless of ambient tail conditions or coordinate system.

These three events display a transition from a relatively undisturbed current sheet to a well-developed, reconnecting current sheet. The thinnest current sheet (Event #1, labeled t_1 in Figure 4) displays weak perpendicular electron heating and no ion heating (Fig. 4a,c). However, as the process develops (Event #2, labeled t_2 in Figure 4), $T_{e,\parallel}$ and $T_{i,\perp}$ increase with respect to $T_{e,\perp}$ and $T_{i,\parallel}$. The current sheet thickness (Fig. 4e) and E_N also increase. Eventually (Event #3, labeled t_3 in Figure 4), the temperature anisotropy and current sheet thickness of "electron-only" reconnection become consistent with the thickness and anisotropy of well-developed reconnection in the near-Earth magnetotail (Fig. 4b,d,f). Importantly, in the furthest developed example of "electron-only" reconnection (Event #3, t_3), $T_{i,\parallel}$ appears to strongly exceed $T_{i,\perp}$ close to the current sheet center (Fig. 4c). This feature is also seen in well-developed reconnection (Fig. 4d).

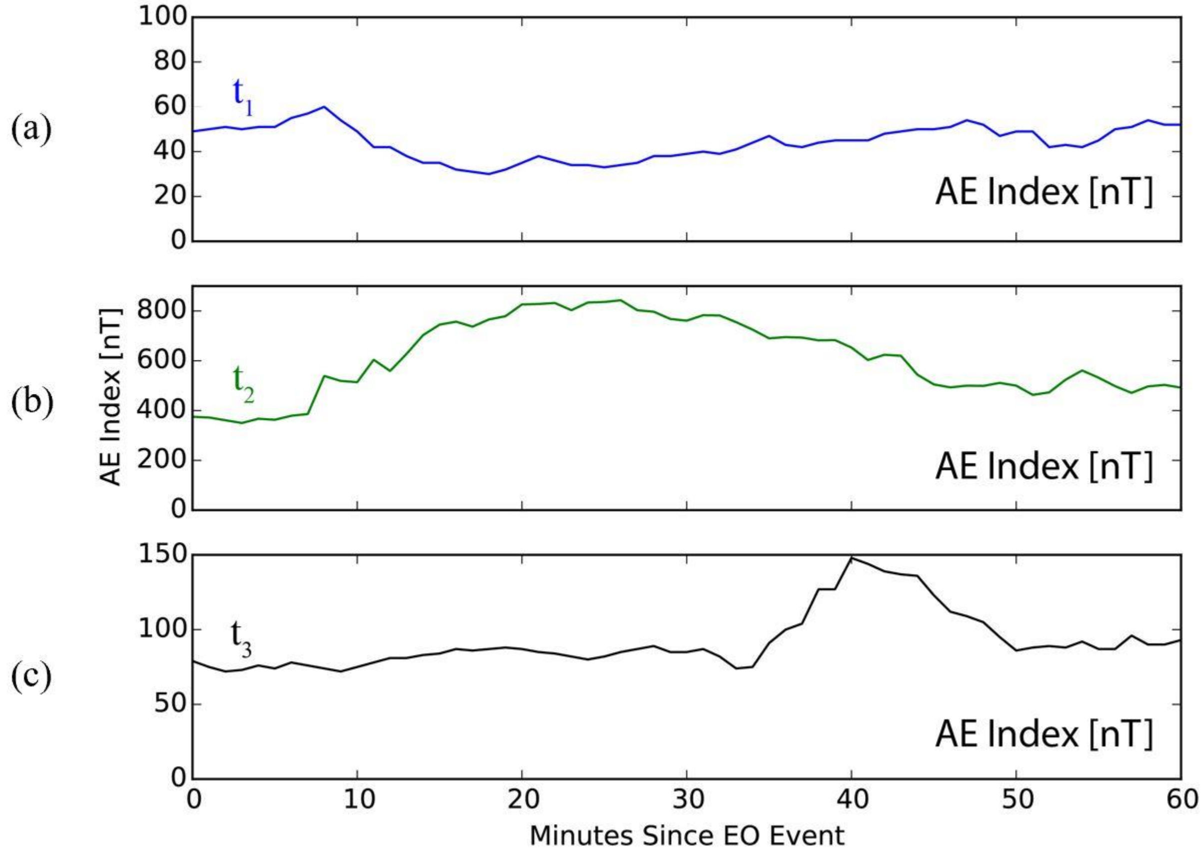

Figure 4: (a) AE Index values for Event #1 (t_1, Blue), (b) for Event #2 (t_2, Green), (c) and for Event #3 (t_3, Red) up to one hour following each Electron-Only observation.

5 Discussion

During the current sheet crossings in Events #2 (2 seconds) and #3 (6 seconds), we observe a static current sheet normal speed and symmetric electron velocity profile. Thus, we argue that "pre-ion reconnection" electron-only events are approximately time stationary over the timescale of these events. This implies that "pre-ion reconnection" events should grow on a timescale that well exceeds 10 seconds. We also note that as electron-only reconnection develops in time, its perpendicular electron crescent (Fig. 1l, Fig. SM1,2) becomes centered at higher energies. This is consistent with the picture that, over time, electrons and ions with larger and larger gyroradii can start to participate in the reconnection onset process.

Oddly, in Figure 4a, Event #1 (t_1) displays mild perpendicular electron heating at the current sheet center. This is the only "pre-ion reconnection" event that displays perpendicular heating. Past simulation work [Dahlin et al., 2014] has shown that betatron acceleration due to ∇B drift can heat electrons located near the cores of X-lines in the perpendicular direction during the early stage of low guide field, symmetric magnetic reconnection. However, this perpendicular electron heating is quickly surpassed by parallel electron heating due to parallel electric fields and Fermi reflection. Thus, we argue that weak perpendicular electron heating early in the "electron-only" reconnection process is plausible. We also note that Event #3's current magnitude is significantly weaker than Event #1 and 2's current magnitudes. With that said, if we normalize each perpendicular current profile by its corresponding electron density, the perpendicular current strengthens from Event #1 (t_1) to Event #2 (t_2) to Event #3 (t_3). Lastly, all three "pre-ion reconnection" events in Figure 4 contain a thick (~20 d_e) region close to the current sheet center in which the electrons are isotropic. While well-developed reconnection also displays this feature, it occurs in a notably thinner (~5 d_e) region. The process that would reduce the size of this region is a subject for future study.

Consistent solar wind and geomagnetic features of "pre-ion reconnection" electron-only reconnection observations are worth noting. To investigate solar wind features, we propagated WIND satellite data to the Earth's magnetopause [Lai et al., 2019]. We observe southward IMF B_z turning less than one hour prior to four of five events (Events #2-5), suggesting that magnetic flux was being carried to the nightside during these intervals. We then examined AE index and DST index data from the World Data Center for Geomagnetism in Kyoto over the 6 hours prior to and following each "pre-ion reconnection" observation. The AE index was perturbed significantly within 60 minutes after three of our five "pre-ion reconnection" observations (Events #2,3,5). Given that three events (Events #2,3,5) show coincident southward IMF B_Z turning and AE index response, we argue that "pre-ion reconnection" electron-only reconnection is typically generated by external solar wind triggering and can develop into well-developed reconnection that produces a significant geomagnetic response.

6 Conclusions

In this study, MMS observed 11 events of "electron-only" reconnection, characterized by a B_L reversal, B_{tot} minimum, super-Alfvenic v_{eL}, lack of ion response, electron heating, positive J·E', deviation of $v_{e\perp}$ from $v_{E\times B}$. Five events occurred prior to traditional reconnection, five events occurred after traditional reconnection, and one occurred with no traditional reconnection signature before or after the event. The thicknesses of these current sheets vary from sub-ion scale to ion scale. Isolating three "pre-ion reconnection" electron-only events, we find that electron-only reconnection develops in time into traditional "electron-ion" reconnection with an increase in parallel electron heating and perpendicular ion heating. This anisotropy eventually reaches the scale seen in well-developed reconnection regions. Over time, these current sheets also increase in thickness. These events' durations suggest that this process develops on a timescale that well exceeds 10 seconds. These events also occur less than 60 minutes after southward IMF B_Z turning and prior to geomagnetic response. Our findings provide evidence that electron-only reconnection occurs in a transient fashion and can contribute to the onset of traditional magnetic reconnection in Earth's magnetotail.

Acknowledgments, Samples, and Data

The authors appreciate helpful discussions and suggestions from S. Lu, A. Runov, A. Artemyev, R. Strangeway, and J. Middleton. All MMS data used in this work are available at the MMS Data Center (https://lasp.colorado.edu/mms/sdc/public/). This research was supported by the NASA Magnetospheric Multiscale Mission, in association with NASA contract NNG04EB99C. The work at UCLA was supported through subcontract 06-001 with the University of New Hampshire.

References

Burch, J. L., Moore, T. E., Torbert, R. B., & Giles, B. L. (2015), Magnetospheric Multiscale Overview and Science Objectives. Space Science Reviews, 199(1–4), 5–21. https://doi.org/10.1007/s11214-015-0164-9

Chen, L.-J., Wang, S., Hesse, M., Ergun, R. E., Moore, T., Giles, B., et al. (2019a), Electron Diffusion Regions in Magnetotail Reconnection Under Varying Guide Fields. *Geophysical Research Letters*, *46*(12), 6230–6238. doi:10.1029/2019GL082393

Dahlin, J. T., Drake, J. F., & Swisdak, M. (2014). The mechanisms of electron heating and acceleration during magnetic reconnection. *Physics of Plasmas*, 21(9), 092304. doi: https://doi.org/10.1063/1.4894484

Dungey, J. W., Interplanetary magnetic field and the auroral zone, Phys. Rev. Lett., 6, 47, 1961.

Ergun, R. E., Holmes, J. C., Goodrich, K. A., Wilder, F. D., Stawarz, J. E., Eriksson, S., et al. (2016), Magnetospheric Multiscale observations of large-amplitude, parallel, electrostatic waves associated with magnetic reconnection at the magnetopause. *Geophysical Research Letters*, *43*(11), 5626–5634. doi:10.1002/2016GL068992

Forbes, T. G., Hones, E. W., Bame, S. J., Asbridge, J. R., Paschmann, G., Sckopke, N., & Russell, C. T. (1981), Evidence for the tailward retreat of a magnetic neutral line in the magnetotail during substorm recovery. *Geophysical Research Letters*, *8*(3), 261–264. doi:10.1029/GL008i003p00261

Fu, X. R., Lu, Q. M., & Wang, S. (2006), The process of electron acceleration during collisionless magnetic reconnection. *Physics of Plasmas*, *13*(1), 012309. doi:10.1063/1.2164808

Huang, S. Y., et al. (2018), Observations of the Electron Jet Generated by Secondary 325 Reconnection in the Terrestrial Magnetotail, Astrophys. J., 862(2).

Lai, H. R., Russell, C. T., Jia, Y. D., & Connors, M. (2019). Magnetized dust clouds penetrating the terrestrial bow shock detected by multiple spacecraft. *Geophysical Research Letters*, *46*(24), 14282-14289. doi: 10.1029/2019GL085818

Li, X., Wang, R., Lu, Q., Hwang, K.-J., Zong, Q., Russell, C. T., & Wang, S. (2019), Observation of nongyrotropic electron distribution across the electron diffusion region in the magnetotail reconnection. *Geophysical Research Letters*, *46*(24), 14263–14273. doi:10.1029/2019GL085014

Lindqvist, P.-A., Olsson, G., Torbert, R. B., King, B., Granoff, M., Rau, D., et al. (2016), The spin-plane double probe electric field instrument for MMS. *Space Science Reviews*, *199*(1), 137–165. doi:10.1007/s11214-014-0116-9

Mallet, A. (2020), The onset of electron-only reconnection. *Journal of Plasma Physics*, *86*(3), 905860301. doi:10.1017/S0022377819000941

Oka, M., Phan, T.-D., Øieroset, M., & Angelopoulos, V. (2016), In situ evidence of electron energization in the electron diffusion region of magnetotail reconnection. *Journal of Geophysical Research: Space Physics*, *121*(3), 1955–1968. doi:10.1002/2015JA022040

Phan, T. D., Eastwood, J. P., Shay, M. A., Drake, J. F., Sonnerup, B. U. Ö., Fujimoto, M., et al. (2018), Electron magnetic reconnection without ion coupling in Earth’s turbulent magnetosheath. *Nature*, *557*(7704), 202–206. doi:10.1038/s41586-018-0091-5

Pollock, C., Moore, T., Jacques, A., Burch, J., Gliese, U., Saito, Y., et al. (2016), Fast Plasma Investigation for Magnetospheric Multiscale. *Space Science Reviews*, *199*(1), 331–406. doi:10.1007/s11214-016-0245-4

Pritchett, P. L. (2001), Collisionless magnetic reconnection in a three-dimensional open system. *Journal of Geophysical Research: Space Physics*, *106*(A11), 25961–25977. doi:10.1029/2001JA000016

Russell, C.T., Mellott, M. M., Smith, E. J., & King, J. H. (1983), Multiple spacecraft observations of interplanetary shocks: Four spacecraft determinations of shock normals, *J. Geophys. Res*., 88, 4739-4748. doi:10.1029/JA088iA06p04739

Russell, C. T., Anderson, B. J., Baumjohann, W., Bromund, K. R., Dearborn, D., Fischer, D., et al. (2016), The Magnetospheric Multiscale Magnetometers. *Space Science Reviews*, *199*(1), 189–256. doi:10.1007/s11214-014-0057-3

Sharma Pyakurel, P., Shay, M. A., Phan, T. D., Matthaeus, W. H., Drake, J. F., TenBarge, J. M., et al. (2019), Transition from ion-coupled to electron-only reconnection: Basic physics and implications for plasma turbulence. *Physics of Plasmas*, *26*(8), 082307. doi:10.1063/1.5090403

Sonnerup, B. U. O. (1979), Magnetic field reconnection, in Solar System Plasma Physics, 370 edited by L. T. Lanzerotti, C. F. Kennel and E. N. Parker, pp. 45-108, North-Holland, 371 New York.

Stawarz, J. E., et al. (2019), Properties of the Turbulence Associated with Electron-only 373 Magnetic Reconnection in Earth's Magnetosheath, Astrophys. J. Lett., 877(2).

Torbert, R. B., Burch, J. L., Phan, T. D., Hesse, M., Argall, M. R., Shuster, J., et al. (2018), Electron-scale dynamics of the diffusion region during symmetric magnetic reconnection in space. *Science*, *362*(6421), 1391–1395. doi:10.1126/science.aat2998

Vega, C., Roytershteyn, V., Delzanno, G. L., & Boldyrev, S. (2020), Electron-only Reconnection in Kinetic-Alfvén Turbulence. *The Astrophysical Journal*, *893*(1), L10. doi:10.3847/2041-8213/ab7eba

Wang, G. Q., Zhang, T. L., Wu, M. Y., Schmid, D., Cao, J. B., & Volwerk, M. (2019), Solar wind directional change triggering flapping motions of the current sheet: MMS observations. *Geophysical Research Letters*, *46*(1), 64–70. doi:10.1029/2018GL080023

Wang, R., Lu, Q., Nakamura, R., Baumjohann, W., Huang, C., Russell, C. T., et al. (2018), An Electron-Scale Current Sheet Without Bursty Reconnection Signatures Observed in the Near-Earth Tail. *Geophysical Research Letters*, *45*(10), 4542–4549. doi:10.1002/2017GL076330

Yamada, M., Kulsrud, R., & Ji, H. (2010), Magnetic reconnection. *Reviews of Modern Physics, 82*(1), 603–664. doi:10.1103/RevModPhys.82.603

Zhou, M., Deng, X. H., Zhong, Z. H., Pang, Y., Tang, R. X., El-Alaoui, M., et al. (2019), Observations of an electron diffusion region in symmetric reconnection with weak guide field. *The Astrophysical Journal*, 870(1), 34. doi:10.3847/1538-4357/aaf16f